J Mater Sci (2007) 42:9756–9764
DOI 10.1007/s10853-007-1997-8

# Modelling of grain size transition with alloy concentration in solidified Al–Si alloys

**Xiangdong Yao · Arne K. Dahle · Cameron J. Davidson · David H. StJohn**

Received: 11 October 2006 / Accepted: 17 July 2007 / Published online: 21 August 2007


**Abstract** The transition in grain size with Si content in Al–Si alloys has been systematically investigated by the Cellular Automaton-Finite control Volume Method (CAFVM) to understand the operating mechanisms for this behavior. Three aspects: growth restriction factor (GRF), the chemical driving force (CDF) and the constitutional undercooling ($\Delta T_C$) have been demonstrated to affect the microstructure formation, and among them the $\Delta T_C$ plays the most important role. Furthermore, it is also shown that the surface modification of the nucleant particles by silicon significantly influences the grain formation. However, the combined effects of the investigated factors on the grain size were not sufficiently strong to cause a grain size change similar to that observed experimentally. This implies that there could be other mechanisms that control the transition.

## Introduction

Alloy composition has a significant effect on the size and morphology of equiaxed grains, as well as influencing the columnar-to-equiaxed transition (CET) during solidification [1–4]. The effect seems to be quite complex. It has been reported in Al–Si alloys [5–7] that the grain size first decreases with increasing alloy silicon concentration and then, after approaching a minimum, the grain size increases with further silicon additions. Backerud and Johnsson [5] suggested that a cellular-dendritic transition in the growth of equiaxed crystals is responsible for the transition and they proposed that the transition occurs at a growth restriction factor (GRF) of $\sim$ 20. However this hypothesis is not supported by other experimental observations [6], which show that the equiaxed microstructures for all investigated alloy concentrations are of dendritic morphology. Backerud and Johnsson [5] also proposed another possible mechanism where it is suggested that the sharper dendrite tip in high concentration melts could penetrate through the solute layer in front of the growing tip and then grow very rapidly because of the large undercooling in the constitutional zone. This mechanism also lacks support. Furthermore, a transition in grain size with increased solute content is not observed in Al–Zn and Al–Cu alloy [8] systems when the GRF varies across a large range including 20, and this suggests that the GRF is not the reason, or it is at least inadequate, to explain the grain size transition.

Additionally, Backerud and Johnsson [5] stated that altering the cooling rate had no significant effect on the transition. However, Hutt et al. [9] reported that varying mould preheat temperature (i.e., cooling rate) considerably shifted the transition point. In the present research, the effect of silicon concentration on nucleation from three aspects, e.g. the GRF, CDF and $\Delta T_C$, has been systematically investigated by Cellular Automaton-Finite control Volume Method (CAFVM), to clarify the effect of silicon on grain formation in solidified Al–Si alloys, and to

X. Yao (✉)
School of Engineering, James Cook University, Townsville 4811 QLD, Australia
e-mail: Xiangdong.Yao@jcu.edu.au

A. K. Dahle · D. H. StJohn
CRC for Metals and Manufacturing (CAST), University of Queensland, Brisbane 4072 QLD, Australia

C. J. Davidson
CSIRO – Manufacturing and Infrastructure Technology, P.O. Box 883, Kenmore 4069 QLD, Australia

investigate the possible mechanisms responsible for the transition of grain size. We also developed an analytical model which quantitatively predicts the effect of solute redistribution on the chemical driving force (CDF) and the constitutional undercooling ($\Delta T_C$) for equiaxed nucleation [10]. The relationship between the nucleation undercooling and the silicon concentration used in these calculations is derived from the model developed [10].

## Model description

In order to verify present experimental data, modelling of grain formation has been performed under solidification conditions similar to those in the experiments within graphite crucible by Lee et al. [6] and Dahle et al. [11]. As the complexity of the treatment for modelling with consideration of the effect of convection on microstructure formation during solidification, the present model will not include the contribution of convection. However, as the samples together with the graphite crucible were held at a constant temperature of 800 °C, the natural convection would be very weak to influence the grain formation. In addition, there would be no "chilling crystals" on the wall of mould that could increase the nucleation sites by the convection.

In this specific problem, the finite volume method (FVM) is the best selection of numerical methods for calculation of heat transfer due to the very simple geometry of the casting, and we can just consider half of the 2-dimensional domain for simulation of microstructures. The considered domain is divided into $100 \times 50$ square finite volumes with the side length of each volume, $\Delta x = 500$ μm.

### Heat transfer calculation

The governing equation for heat transfer, including the liberation of latent heat, is given by

$$\rho C_V \frac{\partial T}{\partial t} = \nabla(\lambda \nabla T) + \rho L \frac{\partial f_s}{\partial t} \tag{1}$$

where $\rho$ is the density of the alloy, $C_V$ is the specific heat, $\lambda$ is the thermal conductivity, $L$ is the latent heat of the alloy, $T$ is the temperature, $t$ is the time and $f_s$ is the fraction of solid.

Equation (1) can be rewritten as

$$\rho\left(C_V - L\frac{\partial f_s}{\partial T}\right)\frac{\partial T}{\partial t} = \nabla(\lambda \nabla T) \tag{2}$$

with initial and boundary conditions

$$T|_{t=0} = T_0 \tag{3}$$

$$\frac{\partial T}{\partial x}|_{x=0} = 0 \tag{4a}$$

$$T\Big|_{\substack{x=X_{\max} \\ y=0 \\ y=Y_{\max}}} = T_{air} \tag{4b}$$

where $T_0$ and $T_{air}$ are the temperatures of the melt just before the start of the calculation and the temperature of air around the mould, respectively $\partial f_s/\partial T$ can be calculated from the relationship between $f_s$ and $T$ derived from the models of solute diffusion. For volume $i$, $j$, discretized the governing equation for heat transfer with application of a fully explicit scheme, the new temperature of the volume at the time $t + \delta t$ ($\delta t$ is the time step for calculation), $T^{t+\delta t}$, the old temperature, $T^t$, and the variation of heat, $\delta H$, in the volume during one time-step of $\delta t$, obey the following equation

$$T_{i,j}^{t+\delta t} = T_{i,j}^{t} + \left[\frac{\partial T}{\partial H}\right]_{i,j}^{t} \cdot \delta H_{i,j} \tag{5}$$

### Cellular Automaton (CA) algorithm

A 2-dimensional Cellular Automaton (CA) technique is being used to model the microscopic phenomena such as nucleation and growth. Firstly, each volume is divided into $20 \times 20$ square CA cells, thus resulting in a resolution of $\delta x = 25$ μm. It should be noted that this value is of the order of one secondary dendrite arm spacing and is thus well adapted to the modelling of the extension of grains by branching mechanisms. A small modification of the original CA algorithm has been performed to improve the resolution of microstructure by considering not only the four N, S, W, E nearest-neighbour cells of a site location, but also the four cells in the direction of NE, NW, SE, SW. Therefore, with this small modification to the CA algorithm, the same microstructure predictions as those calculated from the original CA model can be obtained with much fewer calculated CA cells, thus improving highly the computational efficiency and computational time.

### Nucleation

For heterogeneous nucleation, the continuous nucleation model developed by Rappaz et al. [12] is adopted. The

nucleation distribution and the nucleation parameters are defined same as Rappaz et al. [12]. During one time-step, $\delta t$, the temperature of the considered cell decreases by an amount, $\delta T$, and thus the undercooling increases by an amount $\delta(\Delta T)$. Accordingly, the density of new grains which are nucleated in the cell of the liquid metal is given by

$$\delta n = \int_{\Delta T}^{\Delta T+\delta(\Delta T)} \frac{dn}{d(\Delta T')} d(\Delta T') \tag{6}$$

Deducing a Gaussian distribution of nucleant potency [12]

$$\frac{dn}{d(\Delta T)} = \frac{n}{\sqrt{2\pi}\Delta T_\sigma} \left\{ \left[ -\frac{1}{2} \left( \frac{\Delta T - \Delta T_{\max}}{\Delta T_\sigma} \right)^2 \right] \right\} \tag{7}$$

where $\Delta T_{\max}$ is the average nucleation undercooling, $\Delta T_\sigma$ is the standard deviation, and $n$ is the density of potential nuclei in the bulk liquid. $\delta n$ can then be calculated by combining Eqs. (6) and (7).

### Growth

As a nucleus appears, it grows according to its growth kinetics. This growth law, $v(\Delta T)$, can be calculated by the KGT model [13]. Then the growth length of the dendrite tip, $L(t)$, during one time step is given by [12]

$$L(t) = \frac{v(\Delta T) \cdot \delta t}{(\cos\theta + |\sin\theta|)} \tag{8}$$

where $\theta$ is the angle of the preferential growth direction, <100>, with respect to the cell horizontal direction. When $L(t)$ is greater than the length of the CA cell, which means that the growing dendrite tip from the solid cell touches the centre of its neighbouring liquid cell, the entrapment of the nearest-neighbouring cell occurs, and the dendrite in this cell grows in the same direction.

### Coupling of macroscopic (FVM) and microscopic (CA) models

The term $\left[\frac{\partial T}{\partial H}\right]^t \delta H$ in Eq. (5) gives the variation of temperature of the nodes of the finite volume during a time step, $\delta t$, and this variation would increase the volume fraction of solid which is calculated quantitatively using the CA model. In each time step, the temperature of each cell which belongs to the finite volume is calculated by using the linear interpolation method. Therefore, the variations of temperature, $\delta T$, of these cells during one time-step, and thus variations of the local undercooling, $\delta(\Delta T)$, are deduced to calculate the variation of the local volume fraction of solid of the cells, $\delta f_{s,cell}$, using microscopic models (nucleation models). The latent heat contribution of each cell is then fed back to the nodal points of the finite volume, also using linear interpolation, in which the interpolated coefficient is a reciprocal of that of the temperature interpolation of the cell. Total contributions to each nodal point of all the cells associated with the nodes of the finite volume would increase the temperature of the nodal point by $\left[\frac{\partial T}{\partial H}\right]^t \delta H$in which $\delta H$ is the sum of total latent heat contributions to each node.

### Calculation of time step

Two time-step schemes, one for macroscopic heat transfer calculation with FVM, $\Delta t \leq \Delta x^2/4\lambda$, and one for microscopic microstructure formation simulation with CA, $\delta t \leq \delta x^2/4\lambda$, respectively, have been used in this simple coupled CAFVM algorithm to reduce computational time.

## Determination of the nucleation parameters

There are no big differences for the most nucleation parameters from those determined in Ref. [14]. Only the nucleant particle density has been changed from $2.06 \times 10^{10}$ to $1.28 \times 10^{10}$, because the calculated results will be compared with experimental data from Dahle et al. [6, 11] which have some differences by Easton and StJohn [15] from which their experimental data was used for determination of the nucleation parameters for grain refinement. For example, the average grain size for pure aluminium is 1,000 μm by Easton but about 1,300 μm for Al-1%Si (the grains should be finer than those for pure aluminium) by Dahle et al. [11]. The difference in the experimental data is reasonable to be accepted because the raw materials of aluminium from different companies may be of different impurity contents. Therefore, it is expected that a less particle density is assumed in the materials used by the experiments of Dahle et al. [11]. The value of $1.28 \times 10^{10}$ can be derived by fitting the calculated result with the experimental data with an Al-3%Si alloy, and it is assumed that the particle density remains unchanged with variation of silicon. Then, this assumption can be tested to be reasonable or not by comparing the calculated and experimental data in Al–Si alloys with 1% and 2% silicon concentrations in which the content of Si is small enough to have no significant effect on the grain size transition according to the experiments. The nucleation site distributions at the mould surface and in the bulk liquid for present calculations are shown in Fig. 1. The growth kinetics is deduced from the KGT model [13], and the investigated levels of the six nucleation parameters in the Gaussian

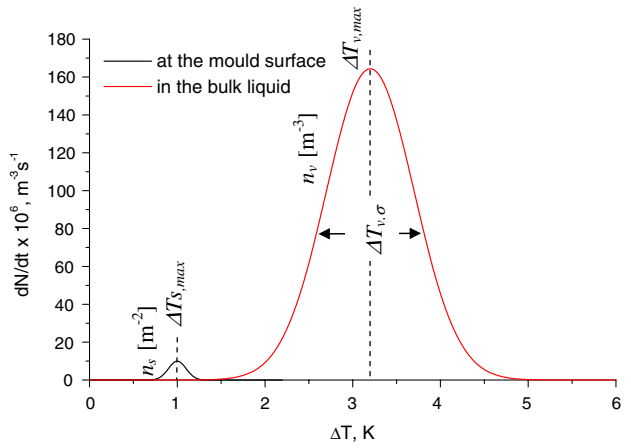


**Fig. 1** Nucleation site distributions at surface of the mould and in the bulk liquid used in the present calculations, $\Delta T_{s,max}$ = 1.0 K, $\Delta T_{v,max}$ = 3.2 K, $\Delta T_{s,\sigma}$ = 0.1 K, $\Delta T_{v,\sigma}$ = 0.5 K, $n_s = 2.5 \times 10^8$, $n_v = 1.28 \times 10^{10}$

nucleation distribution are shown in Table 1 [12, 13]. The thermophysical properties and solidification parameters used in the present calculation are shown in Table 2.

## Results and discussion

### Effect of the GRF

Figure 2 shows predicted microstructures for Al–Si alloys with 1, 2, 3, 4, 5 and 8% Si concentrations. It is readily apparent that the silicon content has a significant effect on grain formation during solidification of Al–Si alloys. The results indicate that the columnar zone decreases rapidly with increasing silicon concentration, which means that the silicon greatly enhances the CET during solidification. Meanwhile, the domain of the equiaxed zone is increased and equiaxed grains become considerably finer with increasing Si. The variation in calculated average grain size and columnar grain length with the silicon concentrations is shown in Fig. 3. Both the average grain size and the length of columnar grains decrease sharply with low levels of silicon concentrations (less than 3%), but this change becomes flat with further higher silicon content. There is a similar tendency to the results for titanium additions studied experimentally by Easton and StJohn [15], which suggests that the silicon has a similar effect on grain formation to that of titanium, but the magnitude of extent is different due to the differing values of the GRF.

The results in Fig. 3 also show that the calculated grain size is considerably different from the experimental data by Dahle et al. [11] because only the effect of GRF on the thermal undercooling (by changing the rate of latent heat released) has been considered. According to the analytical study, however, two other effects of the silicon concentrations on grain formation should be taken into account to properly predict the solidified microstructures: the effect on CDF [10] and effect of the constitutional undercooling. The growth rate varies with the GRF resulting in variation of the solute redistribution ahead of the interface to change

**Table 2** Thermophysical properties of Al–Si alloys[3] and the solidification conditions

| $T_m^{Al}$ (K) | $T_{eut}$ (K) | $C_{eut}$ (wt.%) | $k_0$ (−) |
|---|---|---|---|
| 933 | 850 | 10.77 | 0.117 |
| $\rho$ (kg/m$^3$) | $C_p$ (J/kg K) | $\lambda$ (W/m K) | $m_l$ (°C/%) |
| 2,720 | 1,086 | 192.5 | −6.5 |
| $D_l$ (m$^2$/s) | $D_s$ (m$^2$/s) | $\Delta_{HV}$ (J/m$^3$) | $\Gamma$ (K m) |
| $3 \times 10^{-9}$ | $1 \times 10^{-12}$ | $1.107 \times 10^9$ | $0.9 \times 10^{-7}$ |
| $T^i$ (K) | $T^m$ (K) | | |
| 1,073 | 1,073 | | |

where $T_m^{Al}$—melting point of pure Al; $T_{eut}$—eutectic temperature of Al–Si alloy; $C_{eut}$—eutectic concentration of Al–Si alloy; $k_0$—solute partition coefficient; $\rho$—density of the alloys (assuming no difference between the solid and liquid for the investigated range of concentration); $C_p$—thermal capacity; $\lambda$—thermal conductivity; $m_l$—the liquidus slope; $D_l$—diffusion coefficient in the liquid; $D_s$—diffusion coefficient in the solid; $\Delta H_V$—the latent heat; $\Gamma$—Gibbs-Thompson surface energy; $T^i$—the initial temperature of the melt; and $T^m$—the preheat temperature of the mould

**Table 1** Growth kinetics and nucleation parameters

Growth kinetics: $v(\Delta T) = k_1 \Delta T^2 + k_2 \Delta T^3$ $\quad k_1 = 39.2 \times 10^{-6} \mathrm{ms}^{-1} K^{-2}$, $k_2 = 4.7 \times 10^{-6} \mathrm{ms}^{-1} K^{-3}$

Nuclear law: $\frac{dn}{d(\Delta T)} = \frac{n_0}{\sqrt{2\pi}\Delta T_\sigma} \left\{ \left[ -\frac{1}{2} \left( \frac{\Delta T - \Delta T_{\max}}{\Delta T_\sigma} \right)^2 \right] \right\}$

| $\Delta T_{s,\max}$ | $\Delta T_{s,\sigma}$ | $n_s$ | $\Delta T_{v,\max}$ | $\Delta T_{v,\sigma}$ | $n_v$ |
|---|---|---|---|---|---|
| 0 | 0.1 | $1.25 \times 10^8$ | 3.2 | 0.5 | $1.28 \times 10^{10}$ |

Units: $n_{s,\max}$ (m$^{-2}$), $n_{v,\max}$ (m$^{-3}$), $\Delta T$ (°C)

The site densities, $n_{s,\max}$ (m$^{-2}$), $n_{v,\max}$ (m$^{-3}$), which are listed in this table apply to 3-dimensional geometries. The following stereological relationships were used to deduce the corresponding values, $n^*_{s,\max}$(m$^{-1}$), $n^*_{v.maz}$(m$^{-2}$), for the two dimensional CA calculations

$n_s = (\pi/4)[n_s^*]^2$ and $n_v = \sqrt{\pi/6}[n_v^*]^{3/2}$

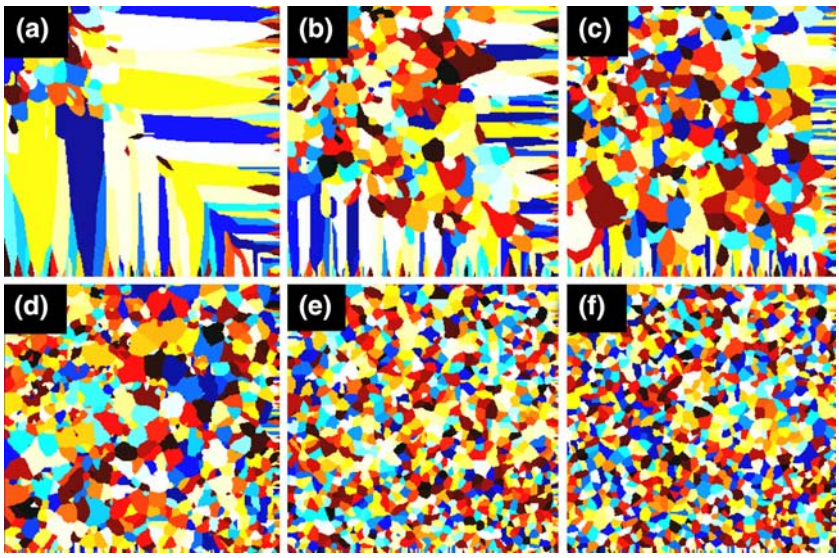


**Fig. 2** Predicted microstructures for Al–Si alloys with 1, 2, 3, 4, 5 and 8% Si concentrations, considering the effect of the GRF

the constitutional undercooling zone. It should be noted that the constitutional undercooling is related to the GRF but can be considered separately when dealing with the nucleation and growth of grains in the remaining melt [10].

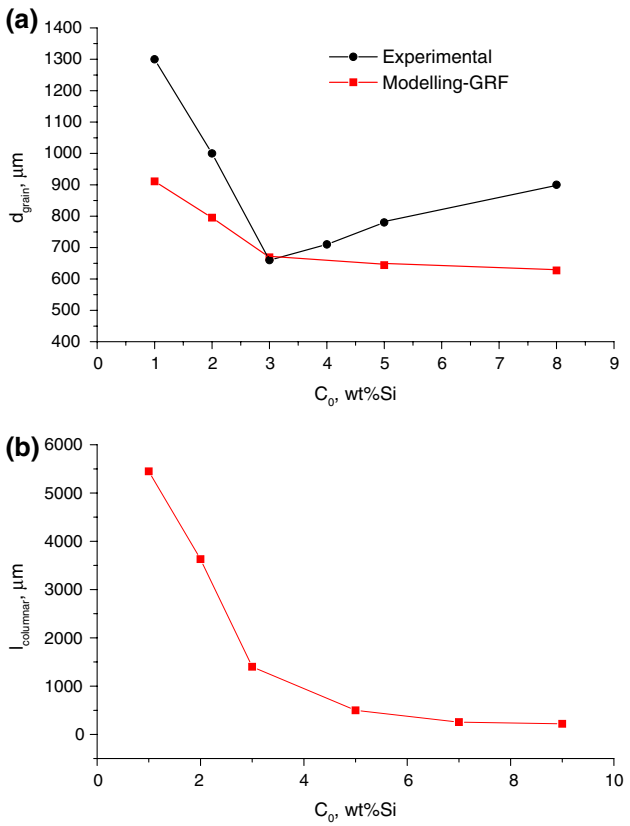


**Fig. 3** Variation of the average grain size (**a**) and the length of columnar grains (**b**) with silicon content of Al–Si alloys, from the model calculation shown in Fig. 2

Effect of the chemical driving force (CDF)

As proposed in Ref. [10], the entropy of fusion, $\Delta S_f$, for liquid/solid phase transformation in Al–Si alloys decreases with increasing the silicon concentration. The CDF for nucleation, $\Delta GV = -\Delta S_f \Delta T$, therefore increases with increased silicon content. Comparing 1% and 9% Si concentrations, there is about 20% difference in the CDF at a given undercooling. Thus, if the potency of a nucleation particle is fixed (that is, properties such as liquid/particle interface energy and the wetting angle do not vary with Si content), a smaller undercooling is required to activate the particle at higher silicon content. This result is shown in Fig. 4 for the nucleation particle characteristics of $\theta_{sl} = 14.4°$, $r_n = 5$ µm and $\sigma_{sl} = 0.1$ J/m$^2$ at the liquidus temperature appropriate to each silicon level, where $\theta_{sl}$ is the wetting angle and $\sigma_{sl}$ is the surface tension between the liquid and the nucleant particle, $r_n$ is the diameter of the particle, respectively. The nucleation undercooling decreases monotonically with increasing silicon content and the difference in the nucleation undercooling between 1 and 9% Si is about 0.45 K.

Assuming that only the mean undercooling of the nucleation site distribution is changed by the calculated nucleation undercooling with the silicon content, the calculated microstructures for Al–Si alloys with 1, 2, 3, 4, 5 and 8% Si concentrations are shown in Fig. 5. The corresponding calculated average grain size and length of the columnar crystals are shown in Fig. 6. It is found that the effect of CDF on the grain size and the columnar zone is not very significant, but it would tend to decrease the grain size with increasing silicon content. The difference between the calculated and experimental data is still considerable and there is no prediction of an increase in grain size about 3% Si.

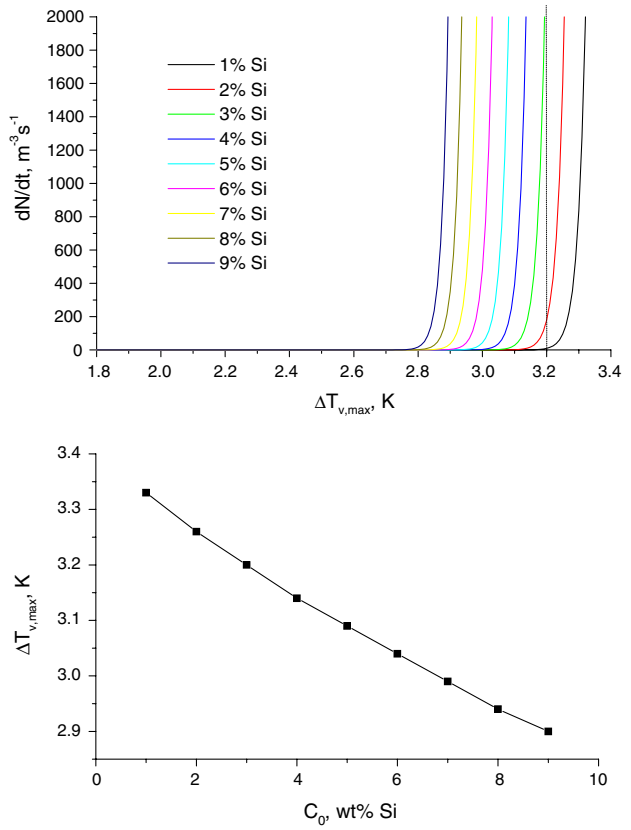


**Fig. 4** Critical undercooling for nucleation with a potential nucleant particle ($\theta_{sl}$ = 14.4°, $r_n$ = 5 μm and $\sigma_{sl}$ = 0.1 J/m$^2$) changes with silicon additions by the effect of chemical driving force

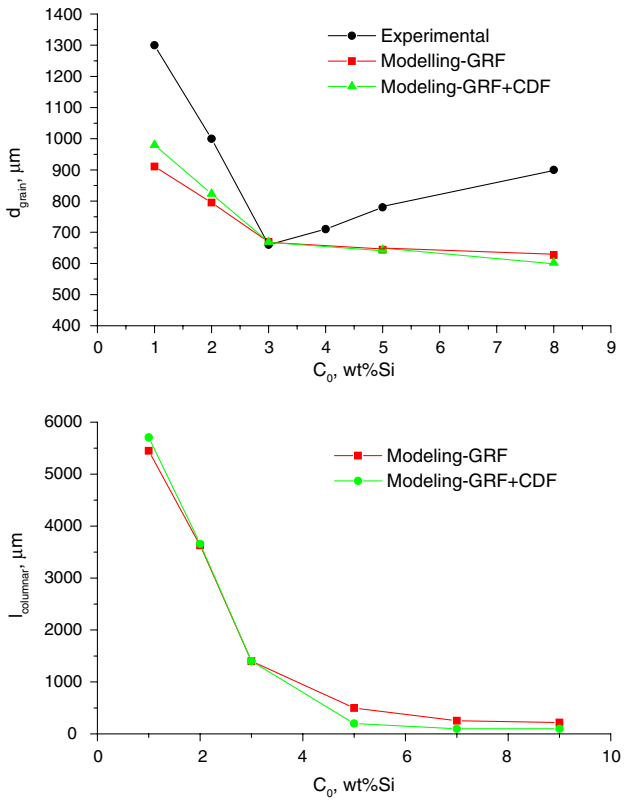


**Fig. 6** Variation of the average grain size and the length of columnar crystals with silicon addition of Al–Si alloys, corresponding to Fig. 5

## Effect of constitutional undercooling

For a given alloy system, the solute redistribution to create the constitutional zone is time-dependent and is influenced significantly by the growth rate. With a high growth rate, the distribution of $\Delta T_C$ is very sensitive to the time, i.e., big difference in $\Delta T_C$ is obtained with a very small variation of time. The time-dependent $\Delta T_C$ can be estimated by the analytical model developed in Ref. [10] for various silicon concentrations, although the actual $\Delta T_C$ is difficult to be accurately in-situ determined during solidification at the

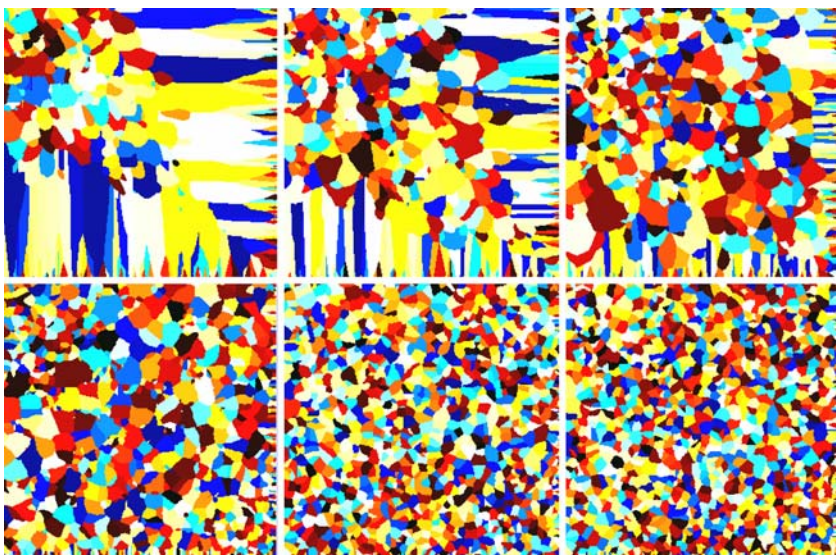

**Fig. 5** Predicted microstructures for Al–Si alloys with 1, 2, 3, 4, 5 and 8% Si additions, considering the combined effect of the GRF and CDF

time of nucleation because the time is hardly determined. The $\Delta T_C$ resulting from the redistribution of the solute silicon for a dilute composition is proportional to the Si content. At a high concentration of Si, it is assumed that the $\Delta T_C$ has no significant change with Si content because the grain size remains unchanged in experimental observations. As the GRF and CDF at a high Si content have a very little effect to decrease the grain size, the variation of $\Delta T_C$ is quite small. Therefore, under the proposed solidification and alloy conditions, it is reasonable to assume that the $\Delta T_C$ keeps almost constant at high Si contents.

Accordingly, in the case of Al–Si alloy solidification, we have inferred from the experimental data of grain size with Si contents, which the $\Delta T_C$ increases linearly with silicon concentration between 0% and 3%, and is independent of Si at concentrations above 3%. On this assumption, only two values of $\Delta T_C$ (at 0% and 3%Si) are required to determine the parameter for all alloys in the range. Keeping other nucleation parameters remain unchanged as given in above calculations, only mean undercooling is changed to calculate the average grain sizes for 0% and 3%Si Al–Si alloys, respectively. The calculated results are then compared with the experimental data. The mean undercooling for the two alloys can be obtained, 4.08 K for 0%Si and 3.2 K for 3%Si of Al–Si alloys, respectively, when the calculated and experimental data are fitted. The difference in the value of $\Delta T_C$ with pure Al and 3%Si is 0.88 K. The values of $\Delta T_C$ with 1% and 2%Si can be obtained by interpolation. The result is shown in Fig. 7. $\Delta T_C$ remains constant when the Si concentration is larger than 3%. In Ref. [10] we have given detailed discussion on the phenomenon of why $\Delta T_C$ does not significantly change above a certain level of solute Si. The value of the $\Delta T_C$ shown in Fig. 7 can be then tested by comparing with the calculated and experimental data for other silicon additions.

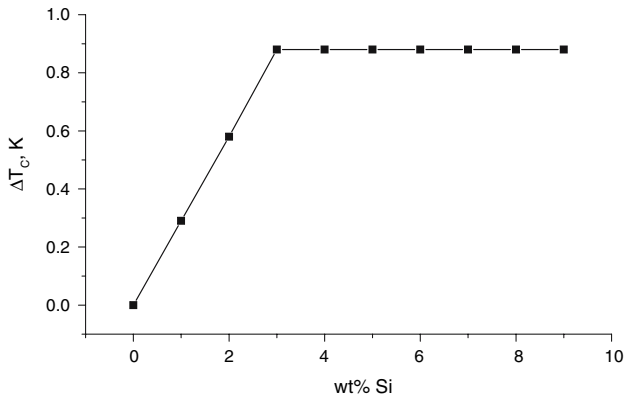


**Fig. 7** Estimation of the constitutional undercooling variation with silicon concentration in Al–Si alloy used in the CAFVM calculation

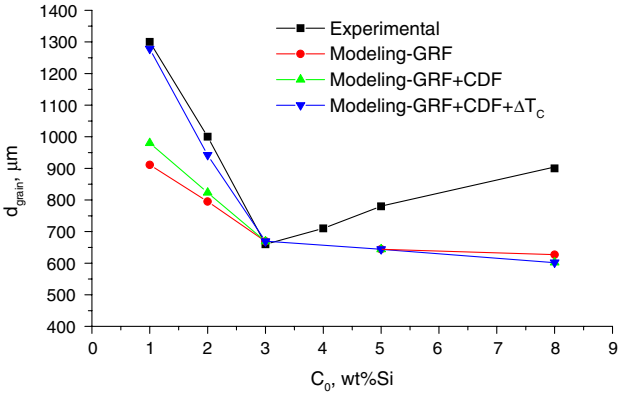


**Fig. 8** Variation of the average grain size with silicon addition of Al–Si alloys, considering the combined effect of the GRF, CDF and $\Delta T_C$

As a result, Figure 8 shows the calculated results for different silicon contents and comparison with experimental data. It is found that the calculated results with consideration of a combined effect of the GRF, CDF and $\Delta T_C$ agree very well with the experimental data for 1% and 2%Si additions. This suggests that the above assumption of the $\Delta T_C$ is reasonable. However, considerable differences between the calculated and experimental data remain for silicon levels above 3%. which is so-called the grain size transition. A possible mechanism will be investigated in the last section.

## Mechanism of the transition of grain size

Three possible mechanisms for grain size transition have been presented. According to Johnsson [16], the grain size begins to increase once again above the critical value, due to a change in the growth mode of the dendrites—diffusion-controlled growth to dendrite tip radius controlled growth. However, little evidence is provided to support this mechanism to explain the transition. Moreover, other alloy systems such as Al–Cu and Al–Zn do not show the transition under similar solidification conditions, which would suggest that variation in dendrite tip morphology resulting by the solute enrichment does not generally cause the transition [8]. Spittle et al. [17] proposed that the potency of nucleation particles decreased by particle surface modification with silicon, thus higher critical undercooling for nucleation was required during solidification. This mechanism has been experimentally supported recently by Lee et al. [6]. Another mechanism was also presented by Johnsson [16] to state that the very sharp dendrite tip could penetrate the solute layer to grow into the undercooling melt, thus the huge growth rate would produce large grains.

In the CAFVM study, Spittle et al.'s hypothesis [17] was tested by firstly assuming that the silicon increases the

nucleation barrier by modifying the nucleation particle surface. The nucleation barrier refers to the mean undercooling of the continuous nucleation model [12] used here. Therefore, all other nucleation parameters can remain unchanged, for calculating grain formation for Al–Si alloys with 3 ~ 9%Si, respectively. The results are shown in Fig. 9. The calculated average grain size can be agreed very well with the experimental data by changing the mean undercooling for the calculations. From the Fig. 9, each mean undercooling for different silicon concentration in the Al–Si system was required as shown in Fig. 10a to fit the experimental data. Accordingly, variation of the wetting angle between particle/liquid interfaces can be calculated as shown in Fig. 10b. Figure 10a shows that the mean undercooling increases with increasing silicon content and is well fitted by an equation shown in the Figure. Figure 10b gives the corresponding wetting angle that would be required in order to generate the fitted mean undercooling values. As the mean undercooling with a high solute concentration is very high, fewer nucleation particles can be activated to form grains and the predicted grain size is large. It should be noted that increased mean undercooling in the continuous nucleation model will increase the extent of the columnar zone during solidification, thus, the mean undercooling can not be sufficiently large to predict the experimental grain size while retaining an equiaxed grain structure. This means that the mean undercooling predicted by Fig. 10a at high Si concentrations is not available for calculating equiaxed grains because no equiaxed grains will be formed. The fact that very good agreement between the calculated and experimental data shown in Fig. 9 is obtained with unrealistic parameters suggests that a second mechanism (unknown) may control the transition for the present solidification conditions, but does not disprove the other two mechanisms.

Calculated results demonstrate that the calculated grain sizes agree well with the experimental data for silicon contents less than 3%. It is suggested that the grain formation in Al–Si alloys lower than 3% Si is controlled by the GRF, CDF and the constitutional undercooling, however, the Si surface modification and the unknown mechanism do not take effect on grain size at this range of Si content. Taken account the GRF, CDF and the constitutional undercooling, and the Si surface modification as well into the calculation, poor agreement as silicon levels increased beyond 3% suggests that the unknown mechanism for the transition besides the particle surface modification by silicon should be the operating mechanism for this unique grain size transition. Although the dendrite tip growth into undercooled melt by penetrating through the solute layer can be simulated by a modified CA algorithm [18], this mechanism seems to be impractical in real solidification, because it is evident that Al–Si alloys solidifying with high nucleant density have a tendency to exhibit a less developed dendrite microstructure [19]. This result also does not agree with the growth mode mechanism proposed by Johnsson [4]. The operating mechanisms for the transition require further investigations.

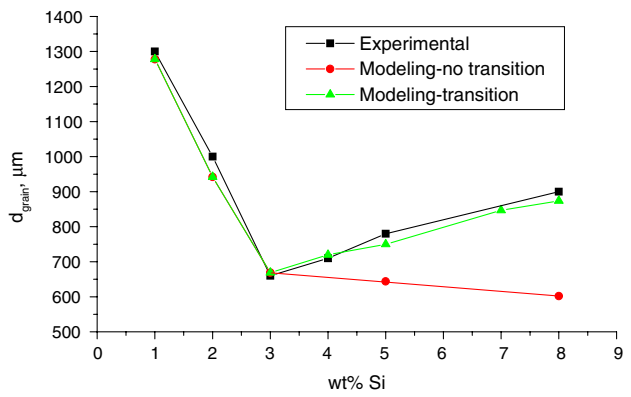


**Fig. 9** The grain size transition in solidified Al–Si alloys

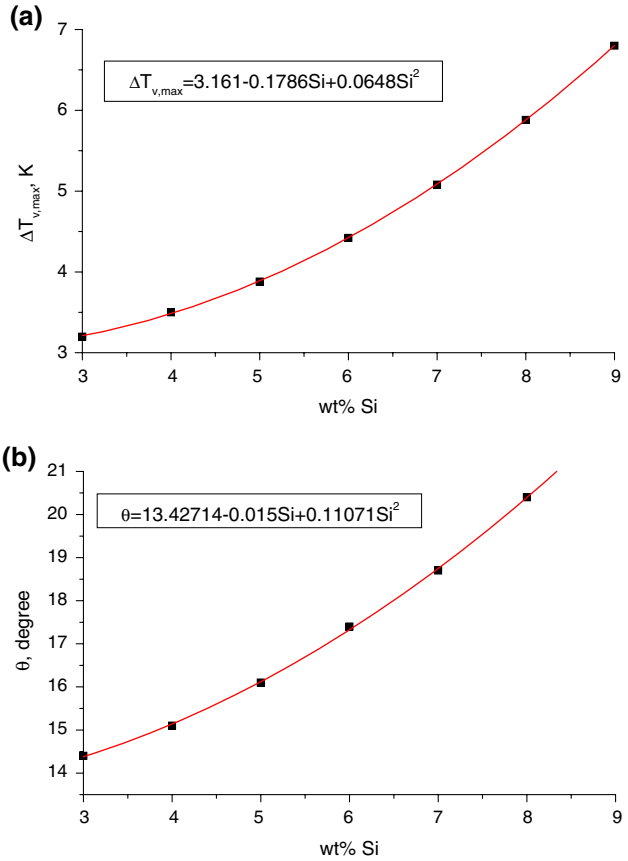


**Fig. 10** Variation of nucleation undercooling (**a**) and the wetting angle between particle/liquid interfaces (**b**) with silicon additions in Al–Si alloys

## Conclusions

Three aspects of grain structure formation have been studied by CAFVM for Al–Si alloy solidification: the GRF (growth-restriction factor); the CDF (chemical driving force); and the constitutional undercooling. The CDF is calculated by the model developed [10] and the constitutional undercooling is estimated from experimental results and the analytical model [10]. It is found all the three factors influence the grain formation during Al–Si alloy solidification but have more significant effect for low silicon contents.

However, no combination of these factors was found that could explain the experimental observations of increasing grain size with Si levels above 3%. The hypothesis that increasing Si modifies the nucleant particle surface to increase the nucleation barrier was tested by modelling. It has been shown that this hypothesis is insufficient to explain the magnitude of the results. This suggests that other mechanisms cause the grain size transition for microstructure formation Al–Si alloys.

## References

1. Flood SC, Hunt JD (1987) J Cryst Growth 82:543
2. Maxwell I, Hellawell A (1975) Acta Metall 23:229
3. Kurz W, Fisher DJ (1989) Fundamentals of solidification. Trans. Tech. Aedermannsdorf, Switzerland
4. Quested TE, Greer AL (2005) Acta Mater 53:4643
5. Johnsson M, Backerud L (1996) Z Metallkd 87:216
6. Lee YC, Dahle AK, StJohn DH, Hutt JEC (1999) Mater Sci Eng A259:43
7. Hutt JE, StJohn DH (1998) Int J Cast Met Res 11:13
8. Hutt JE (2001) PhD Thesis, The University of Queensland
9. Hutt J, StJohn DH, Hogan L, Dahle AK (1999) Mater Sci Technol 15:495
10. Yao X, Dahle AK, Davidson CJ, StJohn DH (2006) J Mater Res 21:3009
11. Dahle AK, Hutt JEC, Lee YC, StJohn DH (1999) AFS Trans 107:265
12. Rappaz M, Gandin Ch-A (1993) Acta Metall 41:345
13. Kurz W, Giovanola B, Trivedi R (1986) Acta Metall 34:823
14. Yao X, Dahle AK, Davidson CJ, StJohn DH, (2000) J Mater Sci (submitted)
15. Easton M, StJohn DH (1999) Metall Trans 30A:1613
16. Johnsson M (1993) PhD thesis, Stockholm University, Stockholm
17. Spittle JA, Sadli S (1995) Mater Sci Technol 11:533
18. Yao X, Wang H, He B, Zhou X (2005) Mater Sci Forum 475–479:3141
19. Yao X, He B, Wang H, Zhou X (2006) Int J Non-Linear Sci Numer Simulat 7:171